

Shock Tubes: A Tool to Create Explosions Without Using Explosives

I. Obed Samuelraj and G. Jagadeesh

1 Introduction

With a view to design structures that are capable of resisting an impulsive load, experimental research has been carried out right from the advent of the space age. The focus on experimental research was primarily due to a poor understanding of material behavior at high strain rates and large loads that are inherent to an actual impact event. A general lack of material models at high strain rates and the absence of computation power as available today, precluded the use of numerical methods to understand this phenomenon.

1.1 Blast Wave Studies on Scaled Models

To design a spacecraft that may be subject to “high-intensity, asymmetric, short duration external pressures”, Menkes and Opat [20] embarked on a basic study to understand the response of beams to impulse loading using sheet explosives. They identified three modes of failure, classified as *Mode I*—large inelastic deformation, *Mode II*—tensile failure at supports, and *Mode III*—shear failure at supports and cap (plug) formation. These failure modes were verified for metal plates by the works of Nurick et al. for circular plates [36]; and later on for square plates [23].

Apart from metals, woven composite plates have been a material of interest for blast wave studies [18]. The failure modes for such composite plates under high-velocity impact loading have also been identified by various researchers. A summary of these may be found in [3] and the failure modes may again be broadly classified into *matrix failure mode*, *fiber tow failure mode*, and *delamination failure mode*.

I. Obed Samuelraj · G. Jagadeesh (✉)
Department of Aerospace Engineering, Indian Institute of Science, Bangalore, India
e-mail: jaggie@aero.iisc.ernet.in

I. Obed Samuelraj
e-mail: obed.isaac@gmail.com

While model studies such as these help in identifying and narrowing down the best possible material for a given type of impulsive loading, predicting the corresponding prototype structure's response requires a reliable scaling law. Such a law is also required to understand and develop blast mitigation strategies and other protective technologies as there is no scope of conducting reliable and repeatable outdoor experiments. All of these studies require a good understanding of similitude theory and its limitations with regard to these experiments.

1.2 Aspects of Scaling

From similitude theory, a recent review of which may be found in [7], it may be understood that scaling a test structure by β for an impulsive load having a very short rise time [34] would require the impulse also to be reduced by the same factor β . The pressure value, however, needs to remain unchanged for both model and the prototype. This means that if one were to simulate the effect of a 1 kg TNT explosion at a stand-off distance of 1 m on a 1 m \times 1 m square plate, the scaled experiment ($\beta = 2$) would have to have a $1/2^3 = (0.125)$ kg TNT explosive at a stand-off distance of 0.5 m from a 0.5 m \times 0.5 m square plate of the same material. The reflected pressures would then be 80 bar for both experiments and the impulses would be 884 Pa-s and 442 Pa-s for the prototype and the scaled experiments respectively. Similarly, the corresponding decay times (t_{blast}) would be 1.74 ms and 0.87 ms.

The underlying assumptions in such a simple geometric scaling law as this are that the structure's response is elastic, its material strain rate effects are negligible, and fracture, or even ductile–brittle transition is completely absent [13].

Elastic regime

Such a scaling law was experimentally validated for both complete and incomplete¹ the geometric scale model response of a cross-ply laminated E-glass/epoxy plate within the elastic regime [32]. For blast loading on metal plates, however, experimental data that validates scaling is scarcely available. Neuberger et al. [22] in their work on rolled homogeneous armor (RHA) steel plates with scaling factors of 2 and 4 show scaling to be valid when most of the dynamic loading is in the elastic regime.

Plastic regime and material strain rate effects

Although this law does not hold when the loading is inelastic and when strain effects are prominent—because the scaling law takes into account the (constant) static yield stress and not the (variable) dynamic one—researchers had carried out experiments to check the veracity of this claim and found mixed results.

Neuberger and Rittel report that the effect of strain rate was barely seen in their experiments [22]. Schleyer et al. [31] had low loading rates in his experimental facility, so he reports that the final deflections for mild steel loaded with a slow rising

¹when all dimensions are not scaled down by a single scaling factor.

pulse (~ 15 ms) at pressures of the order of 1 bar were scalable ($\beta = 0.5$) in the inelastic regime. While the dynamic deflections did not quite scale-up for the inelastic case, the error involved was not high ($<10\%$) and he reports the effect of strain rate to be minimal. However, in the work of Snyman [33], where he reports blast loading on mild steel plates with scaling factors of 1.6 and 2, a discrepancy as high as 35% was noticed for the mid-point deflection when subjected to a blast pulse that would have been around 250 bar having a decay time of 70 μ s. A general consensus for scaling in the inelastic regime is that using the dynamic yield stress in place of static yield stress would be better if the material can be modeled as a rigid perfectly plastic material. This is valid only when the impact energy is absorbed mostly by means of plastic bending and stretching throughout the volume of the material [14]. In other words, this holds only when almost all of the energy is absorbed in the plastic regime rather than the elastic regime.

In addition to this, it is known that the strain rate effects are amplified by β times that of the value in a prototype [13]. Since the dynamic yield strength usually increases with increasing strain rate, the scale model tests would under predict the prototype's response. Thus, the strain rate effects need to be taken into account to obtain some reliable data from model experiments. To this end, Oshiro and Alves [24] and then Kong et al. [17] propose an approach to account for the effect of strain rate. Oshiro and Alves [24] propose the use of a different basis set to implement the scaling—initial impact velocity–dynamic yield stress–impact mass as against the traditional mass–length–time. They show the validity of this approach for scaling factors all the way up to 1000. Kong et al. [17] had recently proposed a method for obtaining the corrected impulse (after accounting for scaling) to be imparted to the structure to factor in the strain rate effects using an appropriate version of the Johnson–Cook plasticity model. This data, which has been validated numerically, is very helpful to decide on the exact amount of impulse that is to be imparted to a model so as to achieve the correct response in a prototype.

Fracture scaling

The reasons for the non-scalability of fracture lie in the fact that the energy stored in the material is a volumetric one, whereas the energy release that occurs, via fracture, is area dependent [4], making it incongruent for scaling to be possible. Thus, the scaled-down models appear to fail at a higher fracture modulus, by a factor β , where $\beta > 1$. Anderson, on the other hand, suggests that it might be due to the limited time available for damage to accumulate in a scaled-down model [1], thus necessitating a higher stress in the model before a fracture occurs. However, if the proportion of energy absorbed by the failed area is very less compared to the elastic and plastic energy contained in the bulk of the material—which can happen in thin plates—the geometric laws have been shown to be valid within experimental error [15], based on some experiments using blunt impactors (traveling at speeds up to 119 m/s) on mild steel plates. Still, there remains further work to be done as the experimental data correlating fracture in a model and prototype is very scarce.

From the above discussion, the importance of considering all these factors while scaling-up the model response may be appreciated. The effects of strain rate partic-

ularly, help show the importance of impulse in any blast–structure interaction study and so this is one aspect which has to be carefully incorporated while carrying out scaled-down experiments in any lab-scale facility where the focus is in acquiring quantitative information.

1.3 Fluid–Structure Interaction (FSI) Effects

Within these broad contours given under scaling, since the scaling law does not take into account the interaction between the load and the structure, the proportion of impulse transferred, and the nature of the loading needs to be preserved. This implies that the ratio of blast pulse duration (t_{blast}) to the natural time period of the plate (T_n) in both model, and prototype has to be retained. Kambouchev et al. [16] had shown that the amount of impulse that is transmitted to the structure depends on the mass of the structure and the impedance of the loading medium. Along these lines, Xue and Hutchinson [38] had shown that all of the impulse in the air is imparted to the structure, whereas this is partial in the case of water. This implies that one cannot use a different loading medium, say water, to simulate an air blast.

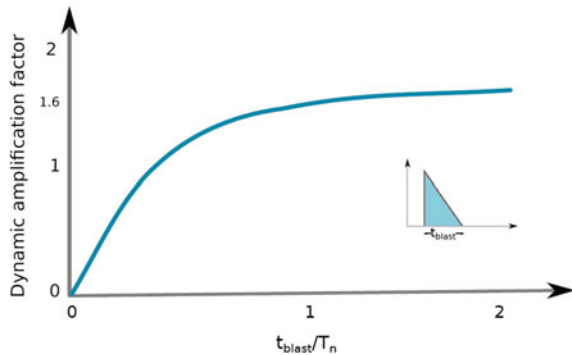
In all of these situations, it is to be recollected that the case of a blast loading and not a gas explosion is being addressed. While blast loading involves extremely short rise times, in the latter case, a finite rise time of the order of a few milliseconds is implied. For this latter case, the ratio of both the rise time and the pulse duration with respect to the natural time period of the structure is to be considered, thus giving us the classic segregation into quasi-static, dynamic and impulse types of loading. For shock loading, however, since the rise time is of the order of microseconds [11], the pulse duration alone is to be considered in order to classify a given loading. While different authors cite different numbers for the limits of the time ratio ($\tau = t_{blast}/T_n$) to determine the type of loading, Li and Meng [19] had come up with some numbers based on the response of a single degree-of-freedom spring–mass model to a blast pulse. Since it is known that the shape of the blast pulse [9] has a serious impact (up to 40% [19]) on the final response, they carried out this analysis for three different types of pulses that have a zero rise time. Such ratios which determine the nature of the loading are provided in Table 1. Since a blast pulse may be considered to be a triangular pulse [2], a shock response spectrum analysis gives the degree to which a single degree-of-freedom system would respond to a given magnitude of load having different t_{blast} durations. Figure 1 plots the ratio of dynamic deflection to the static one versus the time ratio (τ). For the special case $\tau < 0.271$ (cf. Table 1) which constitutes an impulse load, irrespective of the nature of the pulse, as long as the impulse value is the same, the response should not differ. But Xue and Hutchinson had shown that the response to an ideal zero-pulse impulse is the maximum [37], suggesting that the pulse shape does play a role. This perhaps needs to be interpreted in terms of the differing peak pressures of each of those pulses since Jones [13] defines an impulse as a pulse having both a short duration, and a loading pressure that is much higher than its corresponding static collapse load (p_c). Thus, the response

Table 1 Defining ^athe three regimes based on $\tau (= t_{blast}/T_n)$

Type of load	τ_{max} for impulsive regime	τ_{min} for quasi-static regime
Rectangular pulse	0.171	0.402
Triangular pulse	0.211	5.159
Exponential decay	0.275	19.029

^aFrom Li and Meng [19], after incorporating the factor— 2π

Fig. 1 A representative blast wave response curve for a triangular pulse



of a structure is sensitive to the ratio of the loading pressure to the static collapse pressure ($\eta = p/p_c$) as well. This means that as long as the peak pressure is the same and the time duration is short enough to be in the impulsive regime, the responses will be identical. Thus, the magnitude of the pressure load is also important if a blast event is to be recreated.

1.4 Importance of Impulse and Pressure

From the discussion in Sects. 1.2 and 1.3, impulse and pressure, respectively, were shown to be very crucial for the recreation of a blast–structure interaction study. Thus, given a blast event to be recreated, the pressure and a scaled-down impulse value—that has been additionally corrected for (possible) strain rate effects—has to be reproduced. The loading medium also should, preferably, be unchanged.

While small-scale explosives can be used for these experiments, there remain several challenges in terms of getting repeatable results, aligning the charge and detonating it exactly with reference to the model (very crucial as the wavefront is not planar), the associated safety hazards, etc. In view of this, alternate techniques have been explored to carry out these scaled-down experiments. A shock tube being capable of generating a planar wave quite repeatedly—making it easier for numerical modeling—and also being capable of generating a controllable duration of the blast load, it has become a popular device of experimentation for studies on blast wave interaction with structures. While Celander [6] had proposed the use of shock tube

for blast studies on animals back in 1955, it was Stoffel (2001) who first proposed the use of shock tube for impact loading studies on plates. Since then, several researchers have been using the shock tube for blast mitigation and related studies [5, 18, 25, 35].

2 Shock Tubes

A shock tube is a simple device that uses the sudden release of a compressed gas to generate a shock wave. In this section, a description of how a shock tube works and how it may be tailored to generate a blast wave is provided.

2.1 Working of a Shock Tube

The shock tube consists of a high-pressure (driver) and a low-pressure (driven) chamber separated by a diaphragm (Fig. 2) and the shock loading occurs at the far end of the shock tube, where the test plate may be clamped. The rupture of the diaphragm, which for the time being may be assumed to be instantaneous, leads to the formation of a shock wave (an instantaneous pressure rise) that propagates into the low-pressure-driven region and an expansion wave (a pressure drop) that moves at a finite speed into the high-pressure driver side. This expansion fan reflects at the end and then starts propagating into the opposite side, which is now along the direction of propagation of the shock wave. In a typical shock tube experiment, the driver chamber is kept long enough so that this pressure drop (expansion fan) cannot catch up with the shock wave, thus giving rise to a flat-topped pressure pulse at the driven end of the shock tube as illustrated in Fig. 3a. Now, if the test plate were to fail catastrophically after absorbing some impulse from this curve, the pressure would drop rapidly

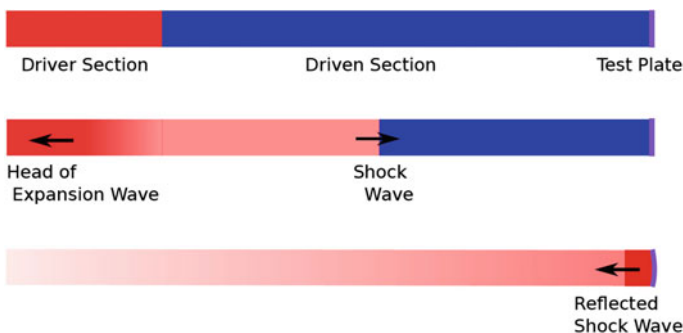


Fig. 2 A schematic drawing showing the working of a shock tube in blast tube mode

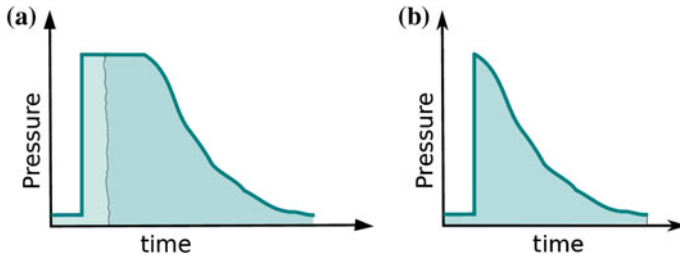


Fig. 3 A typical pressure trace for a shock wave (a) and a blast wave (b). While the pressure pulse in a typical shock tube is as in a, the lengths of the shock tube need to be tailored to obtain b. The first shaded area under the curve in a represents a portion of the impulse that may be absorbed by a structure that fails abruptly

after failure ensues and we would then obtain an extremely short duration pulse as depicted by the left half of the shaded area under the pressure–time curve. But since we are not primarily interested in fracture, we need a pulse with no flat-top region or no dwell time, as in Fig. 3b. To achieve this, we need to tailor the length of the driver side so that this expansion just catches up with the shock wave at the end of the driven chamber.

Using an x-t diagram, where the distance traveled by the wave is shown along the abscissa and the lapsed time is the ordinate, we can better understand the effect of the lengths of the driver and driven sections.

x-t diagram: Figure 4 shows a typical x-t diagram. The shock wave and the contact surface move down the driven section and the expansion wave travels toward the end of the driver section. Once the expansion wave reflects off the driver end wall, it then starts moving along the direction of the shock wave. When the expansion wave catches up with the shock wave after it reaches the end wall, we will have a dwell

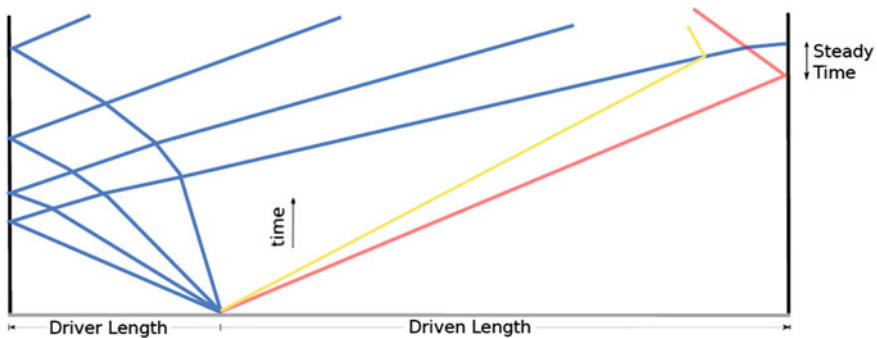


Fig. 4 An x-t diagram showing the shock wave (red), the contact surface (yellow), and the expansion wave (blue). The expansion wave has not caught up with the shock wave before the end wall. It catches up a little later, thus giving a small decay time as in Fig. 3a

time in the pressure trace recorded at the end wall before the decay begins (Fig. 3a). If instead, it catches up with the shock wave either before or just at the end wall, we will have a decaying pressure trace as represented in Fig. 3b. The optimal condition is achieved when it catches up just at the end wall, since an expansion wave catching up earlier would mean a continual reduction in peak pressure until the shock wave reaches the end wall. From the x - t diagram, it is quite clear that we can achieve such a condition, all other parameters remaining unchanged, by making the driven length slightly longer. Assuming that this is done, we next proceed to look at the decay time of the pulse— t_{blast} (cf. inset of Fig. 1). The expansion waves that keep reaching the end wall are the ones that are responsible for decay of the pressure. If we were to assume that three of these “rays” or “fans” are required to bring the pressure down to the ambient value, the longer the length of the driven tube, the longer would be the decay time as may be realized from Fig. 4. This is because these three waves “spread” over time as the tube gets longer, thus delaying the arrival of the final wave. So to have shorter decay times, the driven length needs to be kept short and the driver length would have to be commensurately reduced to obtain a blast profile at the end wall.

But then, a reduction in the driven length is limited by the shock formation distance, which is ultimately proportional to the opening time of the diaphragm, the shock speed, the inner diameter of the shock tube, and the speed of sound in the driven gas [10]. Accordingly, to obtain the shortest possible pulse, the driven length has to be the shock formation distance, and the driver length will then have to be optimized for this driven length.

Gas properties: From the discussion in Sect. 1.3, it is evident that the gas in the driven chamber cannot be different from that in an actual event, which thus has to be *air* for an air blast. On the other hand, the choice of the driver gas is based on gas dynamic considerations of how a shock wave reflects from a contact surface. A contact surface is an interface that separates the shocked gas and the non-shocked gas (*yellow*-colored line in Fig. 4). The reflected shock wave (Fig. 2) would have to cross this interface (which cannot be represented in Fig. 2 as it depicts pressures and not densities) as may be visualized in Fig. 4. If the impedance of the downstream gas is higher, we will have a shock reflection off this interface that would then travel toward the end wall, which is clearly not a desirable condition. So we need to choose a driver gas such that we have an expansion wave reflecting off the contact surface. For the driver pressures that are usually encountered, ~ 20 – 60 bar, the choice falls on helium, which incidentally also gives higher reflected shock pressures for a driver-driven gas pressure ratio.

Test sample: Another important aspect that has to be taken care of is with regard to the mounting of the specimen. Consider the progress of the shock wave once it exits the shock tube. Figure 5a shows a shadowgraph image, an image whose intensity is proportional to the second derivative of density, which can thus highlight a shock wave which is characterized by density jumps. As the image shows, expansion waves that emanate from the corner slowly catch up with the shock wave and progressively weaken the shock wave, thus making the shock nonplanar. Thus, it would be incorrect

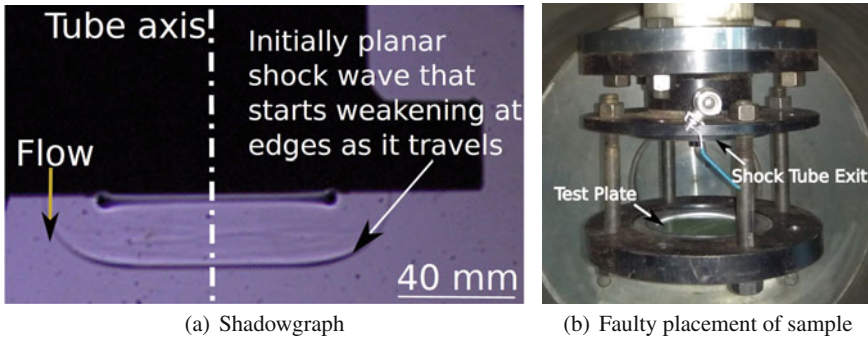


Fig. 5 **a** Shadowgraph image of flow exiting a shock tube. **b** An illustrative photograph that shows the *wrong* positioning of a sample. The gap between the shock tube exit and the sample should ideally be zero

to position the sample at a distance from the exit of the shock tube as shown in Fig. 5b. Instead, the gap between the flange and the sample should ideally be zero so that a planar shock impingement is realized on the sample plate.

3 Shock Tubes at IISc

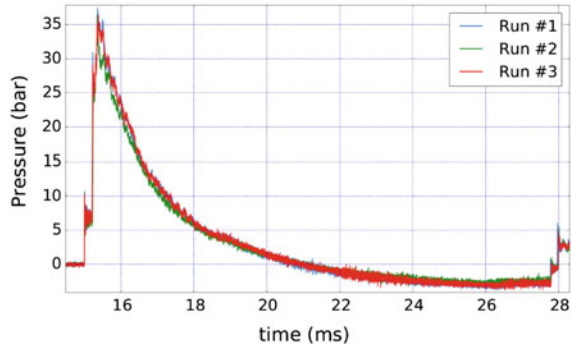
At the Laboratory for Hypersonic and Shock wave Research (LHSR) in Indian Institute of Science, we have shock tubes that are capable of simulating an air blast and an underwater blast event. The following subsections explain each of these facilities, and the work that is usually carried out in them.

3.1 Vertical Shock Tube

A shock tube that has a provision to vary the driver and driven lengths was designed based on the ideas presented in Sect. 2. This facility, a photograph of which is provided in Fig. 6a, has two shock tubes, each with an inner diameter of 136 mm and having a compartmentalized driver section (three tubes of 0.5 m each) and driven section (one tube of 1.5 m, three tubes of 0.6 m, one tube of 0.5 m, and one tube of 0.39 m), thus permitting a good number of combinations of driver and driven tube lengths. The shock tubes have been vertically positioned for ease of carrying out shock impingement studies on a liquid medium. These tubes open into a tank that was primarily intended for noise attenuation and safety purposes. It also has viewing windows to monitor the deformation of the test plate(s).

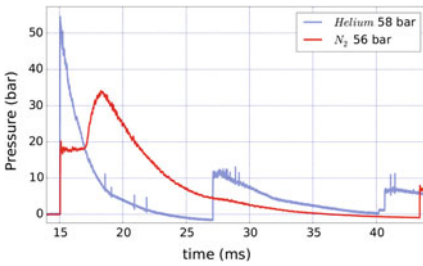


(a) Photograph of the facility

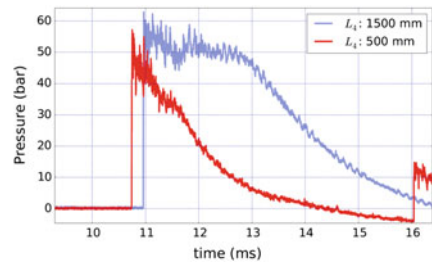


(b) Side-on pressures

Fig. 6 **a** A photograph of the vertical shock tube showing the safety tank and the two variable length shock tubes that sit atop the tank. Three of the five viewing windows may also be seen in this photograph. **b** Side-on pressures measured close to the exit of the shock tube



(a) Different driver gases



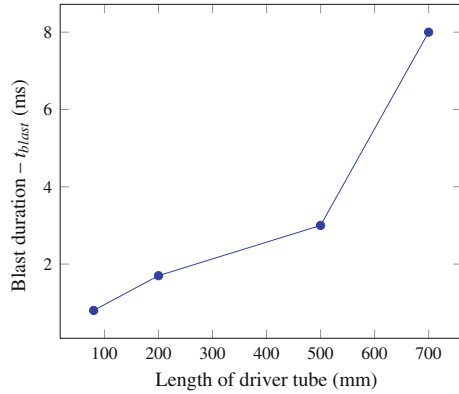
(b) Effect of driver length

Fig. 7 The effect of driver gas and the length of the driver tube on the pulse formation

Figure 6b shows side-on pressures which were measured close to the exit of the shock tube (50 mm) upstream when a rigid concrete block was being loaded by a shock wave generated using $59.3 \pm 2.8 \text{ bar}$ of helium gas. The repeatability in peak pressure was found to be better than 3% and the repeatability in impulse was found to be 4.5%, the wide scatter largely due to the variability in the burst pressures of the metal diaphragm.

As mentioned in the previous section, helium is to be the preferred choice of driver gas. Figure 7a shows what would happen if nitrogen were to be used instead and a demonstrative experiment was carried out using nitrogen at 56 bar, and helium at 58 bar, as the driver gas. The shock tube had a 700 mm long driver and a 4500 mm long driven tube. For the case of nitrogen as the driver gas, we see the shock wave reflecting from off the contact surface as another shock wave, thus giving rise to the second peak, which is clearly to be avoided. The higher reflected pressures that are achieved using helium as the driver gas, for the same driver-driven gas pressure

Fig. 8 An experimental plot showing the effect of driver length on the pulse duration of the blast wave



ratio is also worth being noted. To show the effect of the driver length, consider the plots shown in Fig. 7b. The driver gas used was helium and the burst pressures were $61 \pm 1 \text{ bar}$, and the driven length was 2100 mm. It may be seen that by varying the driver length, with all the other parameters unchanged, we can get either a shock pulse or a blast pulse. Figure 8 further shows how a reduction, or increase in the driver length gave us different blast pulse durations.

For a blast loading test that we carried out on a fully clamped 2 mm-thick Aluminium 6061-T6 plate, a failure that is characteristic of an impulse load was recorded when the pressure loading conditions were similar to the helium signal shown in Fig. 7a. A photograph of the failed sample is given in Fig. 9a. Side-on pressure sensors on the shock tube were mounted at two locations, one each, before and after the plate. The signal is not clean perhaps due to noise in the cables, but it shows that the aluminum plate took about 700 μs to rupture. A correlation with a high-speed

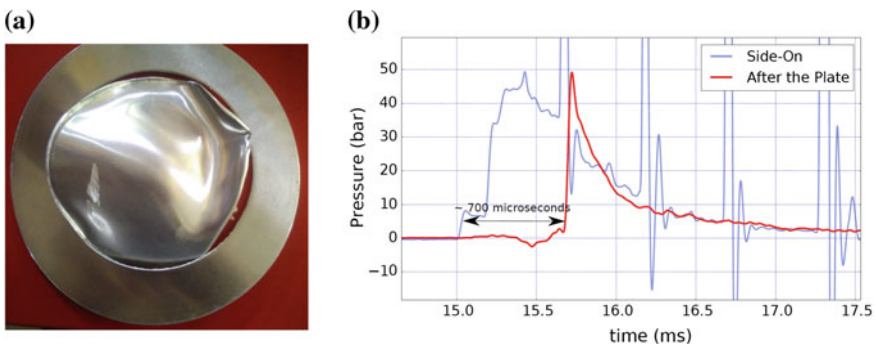


Fig. 9 **a** A photograph showing a 2 mm-thick Al 6061-T6 plate (Φ 136 mm exposed area) that showed an impulse failure and **b** A typical pressure signal showing the side-on pressure from sensors that were placed on the tube. The first signal was from a sensor that was 50 mm above the plate and the second one was at 40 mm after the plate

image recording will help us obtain an exact idea of how the failure had occurred. We had also carried out experiments on a 0.8 mm-thick copper plate and it also showed an impulse type of failure [29]. The experimentally measured impulse value matches well with the impulse value reported in existing literature for this type of failure mode. Since the data in the literature is from small-scale explosive-based experiments, it shows that a shock tube is certainly a capable device for recreating small-scale explosions.

3.2 Automated Shock Tube

For accurate control over experiment, the use of diaphragms is to be eliminated as their variable burst pressures are a major source of uncertainty in any meticulously executed experiment. The use of a diaphragmless system, wherein a fast acting valve performs the role of the diaphragm gives the desired control over such an experiment. Figure 10 shows such a facility at the lab, where the fast open valve is located at the left end and the test specimen may be clamped to the tube at the right end. Nagaraja and others [21] had used this facility to study shock wave-assisted metal forming of thin copper plates (0.15–0.5 mm). The reflected shock pressures were less than 5 bar, and a rectangular pulse was obtained at the end of the tube. For this pressure loading, they observed Mode II (impulse) failure for thin aluminum plates and copper plates. It is interesting to note that an impulsive failure was recorded although the pulse was of much longer duration than the natural time period of the plate. This may be attributed to the plate having failed after absorbing the corresponding damage impulse as mentioned in Sect. 2.1 and as illustrated by the shaded portion in Fig. 3a.

3.3 Free-Piston Shock Tube

From the discussion in Sect. 1.2, it is clear that failure cannot be scaled up. But since there is an absence of more experimental data on verifying scalability of fracture for thin plates, some high-pressure experiments were carried out on (composite) plates, with a view to not only understand the material response to shock loading, but also to obtain data for code validation. In this section and the subsequent one, we describe two facilities that are capable of generating high pressures—one for air blast and the other one for UNDEX.

Free-piston shock tube [27] uses the compressive action of a freely moving piston to heat up the driver gas (helium) adiabatically. This hot gas (up to ~1600 K) which is also at high pressure (~100 bar), bursts a diaphragm, giving rise to high reflected shock pressures. Tailoring the driver length is not an easy task in this device as the piston continues to move even after the rupture of the diaphragm. This facility, thus, generates a shock wave (like the automated shock tube) rather than a blast wave and it was used by Reddy and Madhu [26] as it is capable of generating high pressures.

For experiments on this tube, it was assumed that FSI effects are negligible and so argon, rather than air, was used as the driven gas to achieve higher reflected shock pressures.

FRP plates (courtesy of Defence Metallurgical Research Laboratory (DMRL), Hyderabad) that were 3 mm thick were tested by clamping them between two flanges and placing them at the end of the shock tube. Various patterns of failure were observed as we increased the loading pressure from 70 bar to 200 bar by increasing the initial pressure in the driven section (Fig. 11).

3.4 Liquid Blast Tube

To generate high pressures of the order of tens of MPa, a fast moving piston that hits a water surface may be used to generate a blast wave [8]. This may be used to simulate an UNDEX event.

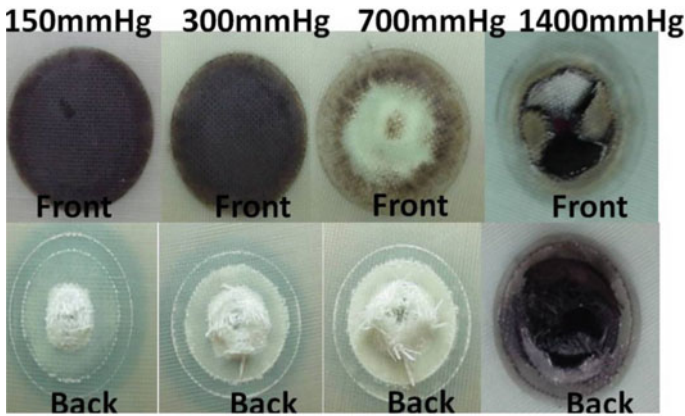
As the piston hits the surface of the water, momentum is transferred to water, and so an elastic wave is generated in the water that travels at the speed of sound in water (~1400 m/s). The initial velocity of the piston is thus imposed on the water at the boundary. Since water is nearly incompressible, it resists the motion of the piston, thereby decelerating it. Thus, the velocity of the piston, and that of the water interface keeps reducing. This leads to a drop in the pressure of the wave that propagates in the water, giving a decaying pressure profile, that is exponential in nature. The peak pressure (p_0) of this wave is related to the density of the liquid (ρ), the speed of sound in the liquid (a), and the velocity of the piston hitting the water interface (v_p) by the



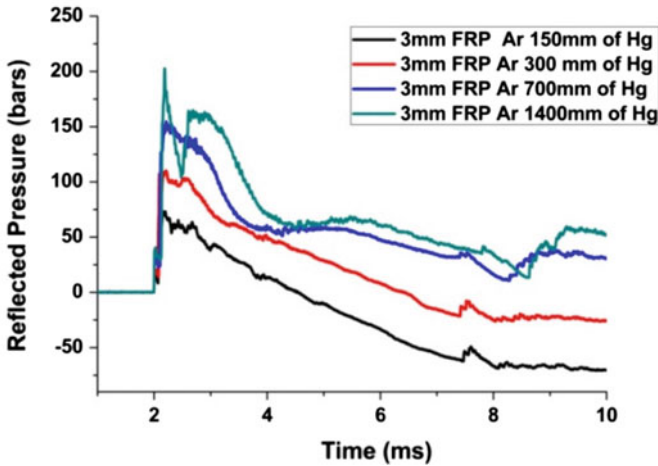
Fig. 10 A photograph of the diaphragmless shock tube at IISc. The inset at the lower right shows failed aluminum and copper samples. The loading area was ϕ 50 mm

Eq. 1. Similarly, the time constant of decay for the blast wave (τ) is related to the mass of the piston (m_p), the cross-sectional area of the piston or the shock tube (A), and the acoustic impedance of the medium (ρa). The cross-sectional area was not explicitly included in [8]. The correct relation is Eq. 2.

$$p_0 = \rho a v_p \tag{1}$$



(a) Damaged composite plates



(b) Reflected shock pressures

Fig. 11 a Blast testing of 3 mm thick FRP plates showing different patterns of damage that were observed as we ramped up the loading pressure. The loading area is Φ 50 mm. The pressures mentioned above each sample refer to the initial pressure of the driven gas. b The reflected shock pressures were measured by a sensor that was flush mounted onto the side-wall of the shock tube near the end

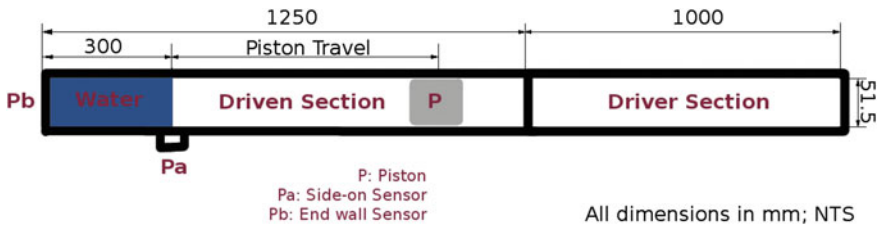


Fig. 12 A schematic diagram showing the major dimensions of the Φ 50 mm vertical shock tube that was used for this experiments. The illustration has been rotated clockwise by 90°

$$\tau = \frac{m_p}{\rho a A} \tag{2}$$

A schematic drawing of the facility has been provided in Fig. 12. A close-fitting piston, made of aluminum, and weighing 0.137 kg was used in these experiments, which was placed at a distance of 500 mm from the diaphragm station. The driver side of the shock tube was filled with water up to the pressure port (P_a), located at ~ 900 mm from the diaphragm, thus giving an effective travel length of about 400 mm for the piston. For the experiments as blast tube, the side-on pressure port (P_a) was left open. This was done both to enable the air that is compressed by the piston to escape and to be used as an inlet to fill the tube with water. The initial pressure rise followed by the exponential decay and the subsequent peak due to the reflection from the end wall of the shock tube may be seen in the experimentally obtained pressure trace (Fig. 13a). Further, it may also be noticed that the rise time is quite significant. This may be attributed to the non-evacuation of the region between the piston and the air–water interface. The air that is being compressed in this intervening region due to the motion of the piston may have contributed to the pressure rise noticed before the peak pressure.

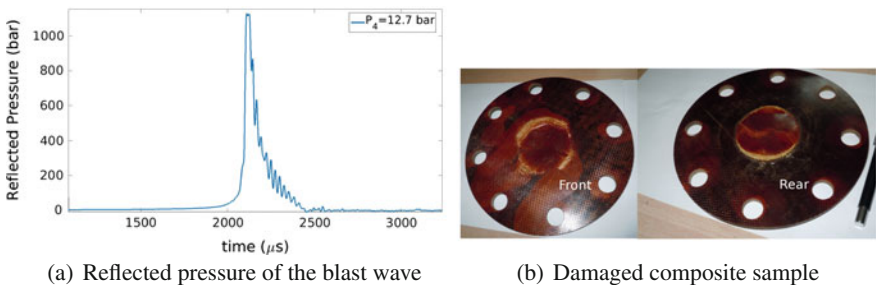


Fig. 13 **a** A typical pressure signal at the end wall of the blast tube. The piston was fired using nitrogen gas at 12.4 bar **b** A photograph of the top and bottom side of the composite plate subjected to an underwater blast. The damaged area is a circle of Φ 50 mm

An E-glass/epoxy composite plate was clamped to the end of this shock tube and was exposed to the shock pressure, a typical signal of which is shown in Fig. 13a. The sample was damaged and exhibited fiber failure as shown in Fig. 13b. As reported elsewhere [28], a delamination type of failure was recorded when the specimen was subjected to a lower pressure.

3.5 Miniature Devices

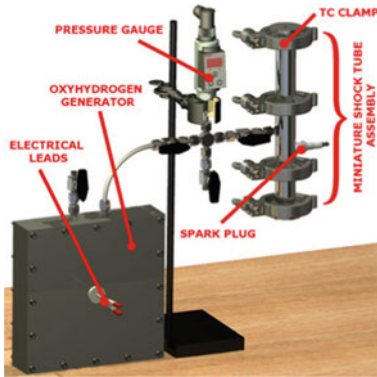
To understand the microstructural response of a material being deformed by a blast wave, samples, whose microstructural and material parameters (stacking fault energy and grain size for a FCC material) have been carefully grown are required. However, samples of such controlled nanocrystalline material may be obtained in bulk only to a maximum size of $\Phi 30\text{--}40$ mm at a thickness of 1 mm, due to limitations in its manufacturing process (pulsed electrodeposition). To study the blast response of such small samples, the use of a miniaturized shock tube was proposed.

Nonel[®] tube: The Nonel[®] tube (M/s Orica Mining Services) is a small plastic tube ($\Phi 3$ mm and 300 mm long) that is coated on the inside with a layer of HMX explosive. On initiating a spark at one end, a detonation wave propagates down the tube, and a high-pressure pulse may be obtained at the other end. We can now clamp a small test specimen onto the other end of this tube using an appropriate fixture and subject it to blast loads that can be as high as 130 *bar* peak pressure. The pressures obtained from this tube were found to be highly repeatable [30], and it has been used for blast mitigation studies elsewhere [39]. But then, the exit pressure of this tube cannot be varied as the tube comes pre-coated with an explosive, which cannot be redone. This led us to develop a new hydrogen–oxygen-based detonation shock tube that was capable of generating repeatable and desired pressures.

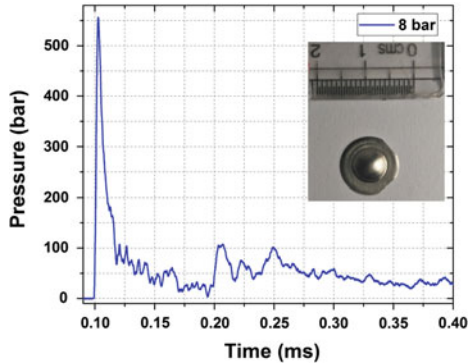
Miniature detonation-driven shock tube: A photograph of this tabletop device is shown in Fig. 14a. The inner diameter of the tube is 6 mm, and the detonation length is 270 mm. A spark plug is located near the center of this tube, and the test plate is clamped to one end of this tube. The other end of this tube is closed. A mixture of hydrogen and oxygen from an in-situ hydrogen–oxygen generator that uses electrolysis of water is filled in the tube and then detonated using a spark plug [12]. A detonation wave is formed once the spark plug is initiated, and this travels down the tube and impinges on the test sample. A typical pressure signal that was obtained at the end wall is shown in Fig. 14b. Since the fill pressure of this shock tube controls the detonation pressure in this device, it is capable of generating repeatable variable shock pressures.

Nanocrystalline Nickel samples ($\Phi 12$ mm) that were 120 and 200 μm thick were tested on these two devices—Nonel tube and the miniature detonation-driven shock tube.

Microstructure studies: Using Nonel tube, nanocrystalline nickel having (200) fiber was deformed and a significant weakening of bulk texture was observed. The forma-



(a) The device



(b) Typical pressure signal

Fig. 14 **a** A photograph of the miniature detonation-driven shock tube and **b** A typical pressure signal at the end of the shock tube. The inset shows a deformed nickel sample

tion of sub-grains was not observed but the grains were highly strained suggesting minimum recovery process which are generally formed in high stacking fault energy FCC metals. The grains were also found to be elongated and shear bands were observed parallel to grain elongation direction. These devices are, thus, being used to carry out basic studies with a view to understand how blast loading can change the microstructure of a material.

4 Summary and Conclusion

The guidelines under which scaled experiments may be carried out were outlined in this work. The importance of matching the pressures and obtaining a pulse duration that is consistent with the geometric scaling laws after incorporating corrections for the strain rate was highlighted in this work. Shock tubes being devices that are capable of generating pressures with extremely short rise times, and fairly repeatable planar waves, with the ability to vary the pulse duration were shown to be invaluable tools in recreating a scaled-blast event. Even if the scale-up of the experiment is not accurate, we may still use this data for validating numerical codes.

The repeatability of 4.5% (impulse) and 3% (pressure) achieved using the vertical shock tube needs to be contrasted against the difficulty in obtaining repeatable experiments using explosives [20], where the repeatability is rarely better than 10%. Based on the shortest duration of 0.8 ms that was achieved on the vertical shock tube, and knowing that a maximum pressure of 100 bar may be achieved on this tube, a 3D graph showing the range and masses of a scaled TNT explosion that can be recreated was plotted in Fig. 15. In this figure, the colored region represents the explosion parameters that may be simulated using this shock tube. While the lower

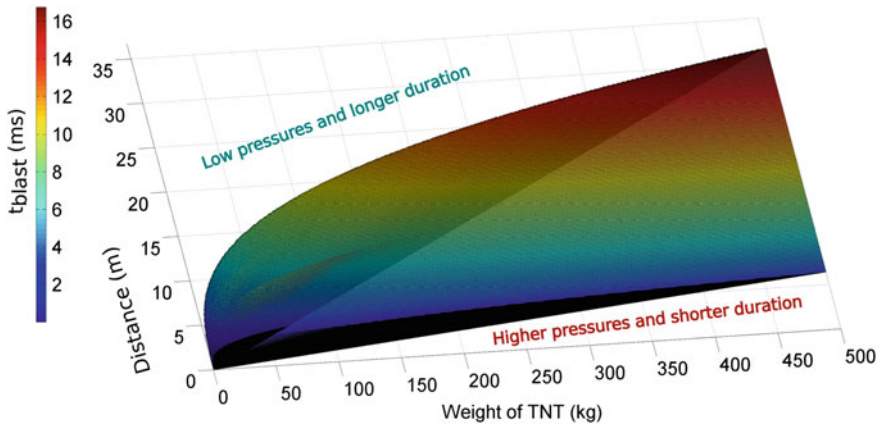


Fig. 15 A 3D plot showing the possible range of TNT weights and distances that may be simulated using the vertical shock tube. The lower and the upper parts including the (*dark*) regions are outside the simulation capability of the shock tube. This graph is for a scaled-down experiment and the corresponding full-scale values may be calculated using an appropriate scaling factor

half represents pressures and decay times that are outside the scope of a shock tube, the upper half corresponds to very low pressures (<2 bar) and longer time durations (>16 ms), which is not of interest for blast interaction with metal plates.

By tailoring the lengths of the vertical shock tube facility, blast wave formation was demonstrated and the diaphragmless shock tube facility may be used to generate repeatable rectangular pulses. These devices were shown to be capable of replicating an impulse failure that has been well documented for small-explosion-based experiments. The liquid blast tube may be used for underwater blast experiments. Finally, we described how a miniature version of a shock tube may be used for a careful study of the effect of shock loading on the grain size and other microstructural aspects of any material.

Acknowledgements We would like to thank the Defence Research and Development Organization (DRDO), New Delhi for funding the research reported in this work. The help received from the staff at the Laboratory for Hypersonic and Shock wave Research (LHSR), IISc is acknowledged with thanks. We also wish to thank Dr. Janardhanraj and Mr. Anuj Bisht of our laboratory, and Mr C J Reddy of DMRL, Hyderabad for sharing some of their data and figures for this article.

References

1. Anderson, C. E. (2003). From fire to ballistics: a historical retrospective. *International Journal of Impact Engineering*, 29(1), 13–67.
2. Anderson, J. C., & Naeim, F. (2012). *Basic structural dynamics*. Hoboken, NJ: Wiley.
3. Ansar, M., Xinwei, W., & Chouwei, Z. (2011). Modeling strategies of 3D woven composites: a review. *Composite Structures*, 93(8), 1947–1963.

4. Atkins, A. (1999). Scaling laws for elastoplastic fracture. *International Journal of Fracture*, 95(1), 51.
5. Aune, V., Fagerholt, E., Langseth, M., & Borvik, T. (2016). A shock tube facility to generate blast loading on structures. *International Journal of Protective Structures*, 7(3), 340–366.
6. Celander, H. (1955). The use of a compressed air operated shock tube for physiological blast research. *ACTA Physiologica Scandinavica*, 33, 6–13.
7. Coutinho, C. P., Baptista, A. J., & Rodrigues, J. D. (2016). Reduced scale models based on similitude theory: a review up to 2015. *Engineering Structures*, 119, 81–94.
8. Deshpande, V., Heaver, A., & Fleck, N. A. (2006). An underwater shock simulator. In: *Proceedings of the Royal Society of London. Series A*, 462, 1021–1041.
9. Fallah, A. S., Nwankwo, E., & Louca, L. A. (2013). Pressure-impulse diagrams for blast loaded continuous beams based on dimensional analysis. *Journal of Applied Mechanics*, 80(5), 051011.
10. Ikui, T., & Matsuo, K. (1959). Investigations of the aerodynamic characteristics of shock tubes. *Bulletin of JSME*, 12(52), 774–782.
11. Jahnke, D., Azadeh-Ranjbar, V., Yildiz, S., & Andreopoulos, Y. (2017). Energy exchange in coupled interactions between a shock wave and metallic plates. *International Journal of Impact Engineering*, 106, 86–102.
12. Janardhanraj, S., & Jagadeesh, G. (2016). Development of a novel miniature detonation-driven shock tube assembly that uses in situ generated oxyhydrogen mixture. *Review of Scientific Instruments*, 87(8):085114
13. Jones, N. (1989). *Structural impact*. New York: Cambridge University Press.
14. Jones, N. (2009). Hazard assessments for extreme dynamic loadings. *Latin American Journal of Solids and Structures*, 6, 35–49.
15. Jones, N., & Kim, S. B. (1997). A study on the large ductile deformations and perforation of mild steel plates struck by a mass—Part II: Discussion. *Journal of Pressure Vessel Technology*, 119(2), 185–191.
16. Kambouchev, N., Noels, L., & Radovitzky, R. (2006). Nonlinear compressibility effects in fluid-structure interaction and their implications on the air-blast loading of structures. *Journal of Applied Physics*, 100(6), 063519.
17. Kong, X., Li, X., Zheng, C., Liu, F., & Guo Wu, W. (2017). Similarity considerations for scale-down model versus prototype on impact response of plates under blast loads. *International Journal of Impact Engineering*, 101, 32–41.
18. LeBlanc, J., Shukla, A., Rousseau, C., & Bogdanovich, A. (2007). Shock loading of three-dimensional woven composite materials. *Composite Structures*, 79(3), 344–355.
19. Li, Q. M., & Meng, H. (2002). Pressure-impulse diagram for blast loads based on dimensional analysis and single-degree-of-freedom model. *Journal of Engineering Mechanics*, 128(1), 87.
20. Menkes, S. B., & Opat, H. J. (1973). Broken beams—tearing and shear failures in explosively loaded clamped beams. *Experimental Mechanics*, 13(11), 480–486.
21. Nagaraja, S. R., Prasad, J. K., & Jagadeesh, G. (2012). Theoretical and experimental study of shock wave-assisted metal forming process using a diaphragmless shock tube. *Proceedings of the Institution of Mechanical Engineers, Part G: Journal of Aerospace Engineering*, 226(12), 1534–1543.
22. Neuberger, A., Peles, S., & Rittel, D. (2007). Scaling the response of circular plates subjected to large and close-range spherical explosions. Part I: Air-blast loading. *International Journal of Impact Engineering*, 34(5), 859–873.
23. Olson, M., Nurick, G., & Fagnan, J. (1993). Deformation and rupture of blast loaded square plates—predictions and experiments. *International Journal of Impact Engineering*, 13(2), 279–291.
24. Oshiro, R., & Alves, M. (2009). Scaling of structures subject to impact loads when using a power law constitutive equation. *International Journal of Solids and Structures*, 46(18–19), 3412–3421.
25. Pankow, M., Justusson, B., & Waas, A. M. (2010). Three-dimensional digital image correlation technique using single high-speed camera for measuring large out-of-plane displacements at high framing rates. *Applied Optics*, 49(17), 3418–3427.

26. Reddy, C. J., & Madhu, V. (2017). Dynamic behaviour of foams and sandwich panels under shock wave loading. *Procedia Engineering*, 173, 1627–1634.
27. Reddy, K. P. J. (2007). Hypersonic flight and ground testing activities in India. In: Peter Jacobs, Tim McIntyre, Matthew Cleary, David Buttsworth, David Mee, Rose Clements, Richard Morgan, Charles Lemckert (Ed.), *16th Australasian Fluid Mechanics Conference (AFMC), Gold Coast, Queensland, Australia*, pp. 32–37, 3–7 Dec.
28. Samuelraj, I. O., & Jagadeesh, G. (2015). *Development of a liquid blast tube facility for material testing*. In: R. Bonazza & D. Ranjan (Eds.) 29th International Symposium on Shock Waves I. Springer, Cham.
29. Samuelraj, I. O., & Jagadeesh, G. (2017). Development of a vertical shock tube facility for blast testing applications. In: *30th International Symposium on Shock Waves* (to be published)
30. Samuelraj, I. O., Jagadeesh, G., & Kontis, K. (2013). Micro-blast waves using detonation transmission tubing. *Shock Waves*, 23(4), 307–316.
31. Schleyer, G., Hsu, S., & White, M. (2004). Scaling of pulse loaded mild steel plates with different edge restraint. *International Journal of Mechanical Sciences*, 46(9), 1267–1287.
32. Simitse, G. J., Starnes, J. H., Jr., & Rezaeepazhand, J. (2000). Structural similitude and scaling laws for plates and shells: a review. *41st AIAA/ASME/ASCE/AHS/ASC Structures, Structural Dynamics, and Materials Conference and Exhibit, AIAA Paper 2000–1383* (pp. A00–24525). GA: Atlanta.
33. Snyman, I. (2010). Impulsive loading events and similarity scaling. *Engineering Structures*, 32(3), 886–896.
34. Sorrell, F. Y., & Smith, M. D. (1991). Dynamic structural loading using a light gas gun. *Experimental Mechanics*, 31(2), 157–162.
35. Stoffel, M., Schmidt, R., & Weichert, D. (2001). Shock wave-loaded plates. *International Journal of Solids and Structures*, 38, 7659–7680.
36. Teeling-Smith, R., & Nurick, G. (1991). The deformation and tearing of thin circular plates subjected to impulsive loads. *International Journal of Impact Engineering*, 11(1), 77–91.
37. Xue, Z., & Hutchinson, J. W. (2003). Preliminary assessment of sandwich plates subject to blast loads. *International Journal of Mechanical Sciences*, 45(4), 687–705.
38. Xue, Z., & Hutchinson, J. W. (2004). A comparative study of impulse resistant metal sandwich plates. *International Journal of Impact Engineering*, 30(10), 1283–1305.
39. Zare-Behtash, H., Gongora-Orozco, N., Kontis, K., & Jagadeesh, G. (2014). Detonation-driven shock wave interactions with perforated plates. *Proceedings of the Institution of Mechanical Engineers, Part G: Journal of Aerospace Engineering*, 228(5), 671–678.